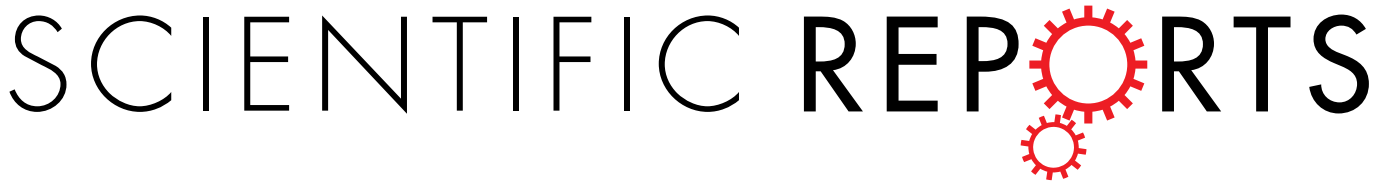

OPEN

Received: 24 August 2015
Accepted: 19 October 2015
Published: 30 November 2015

Porous VO_xN_y nanoribbons supported on CNTs as efficient and stable non-noble electrocatalysts for the oxygen reduction reaction

K. Huang[1], K. Bi[1], Y. K. Lu[2], R. Zhang[1], J. Liu[2], W. J. Wang[3], H. L. Tang[4], Y. G. Wang[1] & M. Lei[1]

Novel nanocomposites of carbon nanotubes supported porous VO_xN_y nonoribbons (VO_xN_y-CNTs) have been synthesized by the annealing of the sol-gel mixture of CNTs and V_2O_5 under NH_3 atmosphere as well as the ageing process in air. Besides the morphological and structural characterizations revealed by TEM, SEAD, EDS, XRD and XPS measurements, typical electrochemical tests including cyclic voltammetry (CV), rotating disk electrode (RDE) and chronoamperometry have been employed to determine the oxygen reduction reaction (ORR) performance of VO_xN_y-CNTs. Inspiringly, the results indicate that VO_xN_y-CNTs catalyst exhibits a 0.4 mA/cm^2 larger diffusion-limited current density, a 0.10 V smaller onset potential value, a 10.73% less of ORR current decay and an excellent methanol-tolerance compared with commercial Pt/C catalyst. Therefore, we have reasonable grounds to believe that this new VO_xN_y-CNTs nanocomposites can be regarded as a promising non-precious methanol-tolerant ORR catalyst candidate for alkaline fuel cells.

With the highly social development of industrialization and urbanization, the critical energy shortages mainly from the depletion of fossil fuels have motivated and accelerated intensive researches in developing alternative energy conversion and storage devices (ECSDs) with higher power and energy densities[1–5]. Among various potential ECSDs for practical applications, polymer electrolyte membrane fuel cells (PEMFCs) have been extensively regarded as ideal power sources for future mobile and stationary applications due to their high energy efficiency, high power density and low level of emissions[6–8]. As important as the biological respiration in life processes, the oxygen reduction reaction (ORR) as the key cathodic process in PEMFCs will determine the behavior of the whole device due to the sluggish kinetics with respect to the anodic electrochemical reactions[9]. Thus, Pt-dominated materials have been used as highly desired catalysts to accelerate the ORR process in order to obtain an enhanced overall performance of PEMFCs. However, the elevated price and extreme CO or methanol sensitivities of the scarce platinum element have limited their widespread use in practical applications, and therefore developing non-precious ORR catalysts with efficient activity and stability has increasingly become the key issue for the commercialization of fuel cells.

Meanwhile, transition metal nitrides and oxynitrides have been intensively researched as suitable electrode or catalyst materials in recent years for various ECSDs, including fuel cells, metal-air batteries,

[1]State Key Laboratory of Information Photonics and Optical Communications & School of Science, Beijing University of Posts and Telecommunications, Beijing 100876, China. [2]School of Materials Science and Engineering, Central South University, Changsha, Hunan, 410083, China. [3]Beijing National Laboratory for Condensed Matter Physics, Institute of Physics, Chinese Academy of Sciences, Beijing 100190, China. [4]State Key Laboratory of Advanced Technology for Materials Synthesis and Processing, Wuhan University of Technology, Wuhan 430070, China. Correspondence and requests for materials should be addressed to J.L. (email: liujun4982004@csu.edu.cn) or H.L.T. (email: thln@whut.edu.cn) or M.L. (email: mlei@bupt.edu.cn)

lithium-ion batteries (LIBs), dye-sensitized solar cells (DSSCs) and electrochemical capacitors (ECs)[10–16], due to the unique physical and chemical properties such as high intrinsic conductivity, relatively good electrochemical stability as well as the Pt-like electrocatalytic activity. And more especially, great interests have also been aroused in the development of vanadium nitrides and oxynitrides as advanced electrode materials by the nitridation of various vanadium oxides precursors. For example, Zhou *et al.* synthesized VN powder by calcining V_2O_5 xerogel under NH_3 atmosphere with a promising supercapacitive specific capacitance of 161 F/g in 1M KOH at 30 mV/s[17]. Glushenkov prepared porous nanocrystalline VN by temperature-programmed ammonia reduction of V_2O_5 powder which exhibited a capacitance of 186 F/g in 1M KOH electrolyte at a current load of 1 A/g[18]. Porto's group investigated the capacitances of VO_xN_y obtained from the nitridation of commercial V_2O_5 and VO_2 precursors with the best specific capacitance of 186 F/g in 1M KOH at 10 mV/s[19]. To further enhance the electrochemical properties of VO_xN_y powders, Chen and his coworker synthesized carbon-supported VO_xN_y nanocrystalline using a mixture of melamine and V_2O_5 xerogel as precursor and obtained a specific capacitance of 273 F/g in 1M KOH at the scan rate of 30 mV/s[20]. Shu *et al.* also developed a soft-template synthesis of VO_xN_y-C nanomaterials for supercapacitors with a maximum specific capacitance of 271 F/g at 1A/g using ploy vinylpyrrolidone (PVP) as the template and V_2O_5 xerogel as vanadium source. Their results demonstrated that the intimate contact between VO_xN_y grains and remaining carbon will result in a better electronic conductivity and the larger surface area will furnish more surface active redox sites[21].

Although the occurrence of fast faradic redox reactions as well as the formation of electrical double-layer on the surface of VN and VO_xN_y have been suggested as the supercapacitive mechanism, few works have yet employed vanadium nitrides and oxynitrides as possible non-precious catalysts towards ORR. Huang *et al.* developed a hydrothermal route followed by calcination to prepare VN powder, which exhibited a comparable diffusion-limited current density but an inferior onset potential to commercial Pt/C catalyst[22]. Our previous work about VN/C catalyst also indicated the same tendency with the addition of the superior stability and methanol-tolerance[23]. Other than loading with Pt particles to obtain an enhanced ORR performance as shown in Yin's work[24], the introduction of porous structure and high surface area supporter can also elevate their electrochemical behaviors due to the increased conductivity and number of active sites[9,25]. Currently, the development of novel multifunctional composites/hybrids by structuring porous materials into the other nanostructures has been regarded as a rapidly developing research area. It is because that the composites/hybrids usually exhibit new properties that are superior to those of the individual components due to the collective behavior of the functional units. Thus, these emerging composites/hybrids will stimulate the emergence of innovative industrial applications in various important fields, including functional and protective coatings, storage and separation, heterogeneous catalysis, sensing and biology[26,27]. Herein, we have successfully synthesized novel CNTs-supported porous VO_xN_y nanoribbons composites with an improvement of structural features as efficient and durable non-precious ORR catalysts in alkaline electrolyte using V_2O_5 nanoribbons and CNTs as raw materials.

Results

Figure 1 shows the morphological characters of as-prepared samples by transmission electron microscope (TEM) equipped with the selected area electron diffraction (SAED). It can be seen that there are plentiful pores distributing in the VO_xN_y nanoribbons due to the topotactic transformation whether supported by CNTs or not (Fig. 1A,D). The high-resolution TEM images show clear lattice fringes with an interfringe spacing of 0.203 nm which corresponds to the d-spacing of (200) planes (Fig. 1C). As for VO_xN_y-CNTs composites, VO_xN_y nanoribbons with a few tens of nanometers in widths and lengths up to micrometer range are randomly supported by plentiful tortuous CNTs (which are more transparent to the electron beam). Moreover, the element mapping spectra visually displayed in Fig. 2 demonstrate the locations of VO_xN_y nanoribbons in the composites. Figure 2B shows the C element from CNTs supporter which distributes everywhere and randomly, while the distributions of V, O and N elements are in accordance with the VO_xN_y nanoribbons to a great extent and the messy existence of O and N elements in Fig. 2C,D is believed to come from the surface species of CNTs. As the XRD patterns shown in Fig. 3, five main peaks ranging from 35° to 85° for both VO_xN_y and VO_xN_y-CNTs can match well with (111), (200), (220), (311) and (222) planes of the typical stoichiometric face-centered (fcc) VO (JCPDS No. 75-0048) or VN (JCPDS No. 73–0528) structures, where the figure of merit (FOM) values are 1.2 and 5.6 respectively. This result can be ascribed to the penetration of oxygen atoms into the VN crystal lattice[17], which happened once the prepared samples were taken off from the furnace. Moreover, the broad peak for VO_xN_y-CNTs sample appears at about 26° which corresponds to the (002) plane of graphite carbon (JCPDS No. 75–1261) and confirms the existence of CNTs.

XPS analysis in Fig. 4 further reveals that the components of VO_xN_y and VO_xN_y-CNTs are consist of V, N, O, and C elements from the survey spectra. Compared with the high intensity peak of CNTs in VO_xN_y-CNTs nanocomposites, it is notable that the signal of C 1S peak for pure VO_xN_y nanoribbons can be attributed to the air contamination on surface[28], which exhibits a symmetric peak at 284.8 eV (Fig. 4D). Figure 4B shows the high-resolution XPS spectra of O 1s and V 2p, where two peaks at 514.2 V (2p 3/2) and 521.5 eV (2p 1/2) can be ascribed to vanadium atoms in the VN crystalline, other four vanadium-based peaks at 515.7, 517.3, 523.4 and 525.1 eV are belong to vanadium oxides and the peaks at 532.2 and 530.3 eV of O 1s can be attributed to lattice oxygen in V_xO_y due to the ageing process

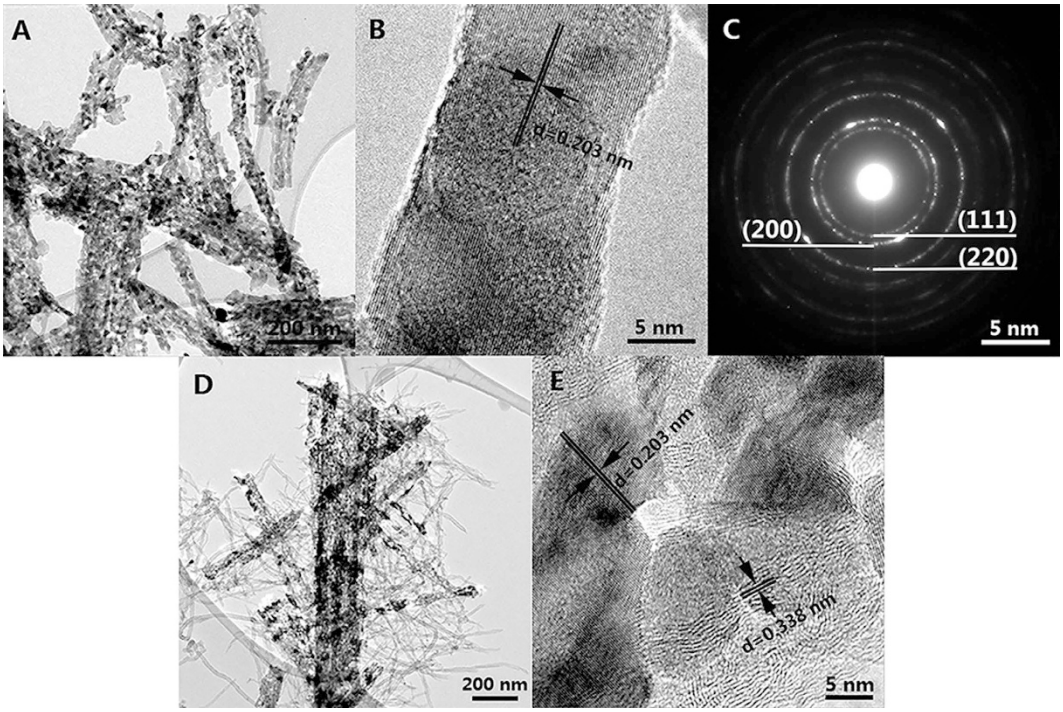

Figure 1. TEM images at different magnifications of VO_xN_y (A and B) and VO_xN_y-CNTs (D and E); SAED image (C) of VO_xN_y-CNTs.

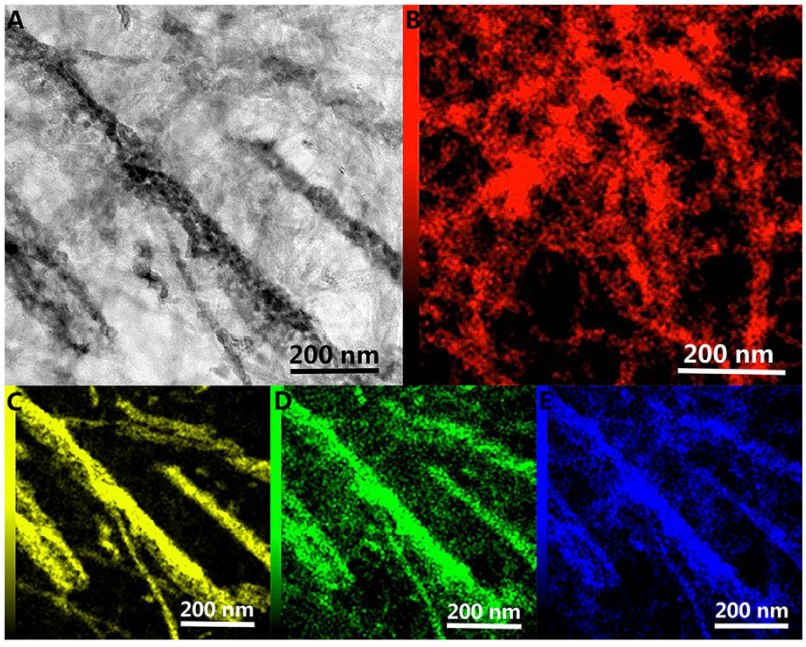

Figure 2. TEM image (A) and element mapping spectra about C (B), V (C), O (D) and N (E) of VO_xN_y-CNTs.

in air and surface adsorbed hydroxyl oxygen, respectively[29–33]. In addition, it is found that the chemical states of N and C elements for VO_xN_y-CNTs are quite different from pure VO_xN_y nanoribbons as shown in Fig. 4C,D. The peak of N 1s spectra at 397.5 eV can be assigned to the corresponding metal nitrides while the other two peaks at 399.5 and 401.3 eV are belonging to pyrrolic and quaternary-graphitic separately[31]. The C 1S spectrum also exhibits a typical aromatic C-N coordination in a graphitic carbon nitride framework at 288.2 eV except for the non-oxygenated ring C (284.8 eV, C-C, C = C) as well as the C-O bond at 286.3 eV[34,35]. These results indicate that a surface modification and N-doping of CNTs

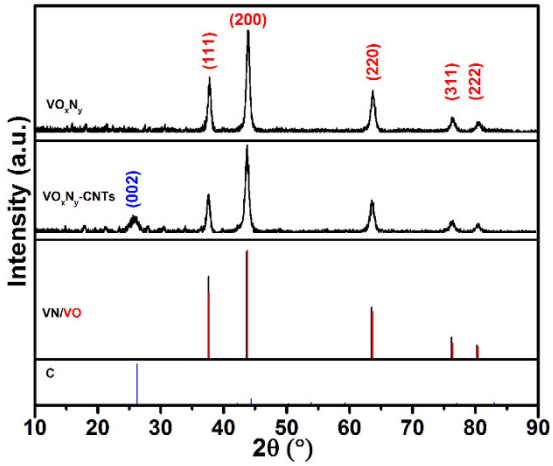

Figure 3. XRD Patterns of VO_xN_y and VO_xN_y-CNTs with the standard patterns of VN, VO and graphite carbon.

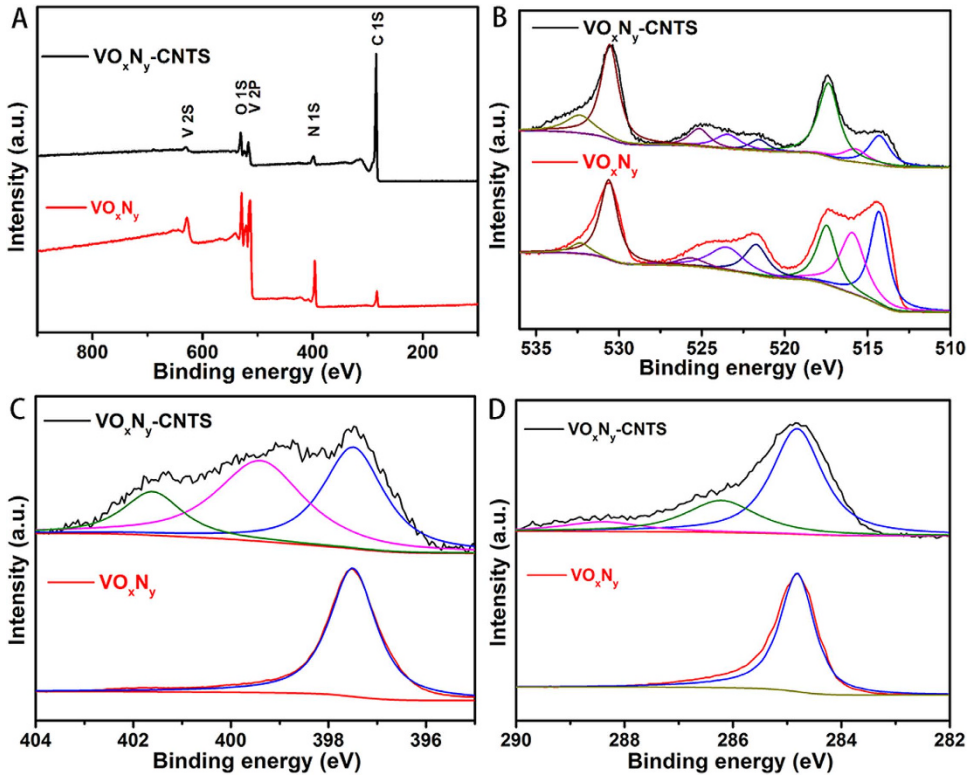

Figure 4. XPS spectra of VO_xN_y and VO_xN_y-CNTs: survey (A), O 1s and V 2P (B), N 1S (C) and C 1S (D).

happened sequentially during the acid treatment and annealing process, which have been proved to show excellent ORR activity[36–38].

The ORR performances of VO_xN_y and VO_xN_y-CNTs catalysts with VO_xN_y-XC 72R and commercial Pt/C as the references have been further investigated in alkaline electrolyte. As shown in Fig. 5, the ORR polarization curves for all kinds of catalysts at 1600 rpm in O_2-saturated 0.1 M KOH exhibit a combined kinetic-diffusion control of charge transfer and mass transport process at different potentials. It is obvious that the support of carbon can improve the onset potential, half-wave potential and the diffusion-limited current density of pure VO_xN_y nanoribbons catalyst, and the hybrid with CNTs displays the strongest competitiveness with respect to the commercial Pt/C. Although the onset potential (0.88 V Vs. RHE) and half-wave potential (0.77 V Vs. RHE) of VO_xN_y-CNTs are 0.10 and 0.07 V smaller than those of Pt/C electrode, the diffusion-limited current density is about 0.4 mA/cm^2 larger. Meanwhile, the stabilities of VO_xN_y-based electrodes are quite superior to that of Pt/C electrode no matter whether adding

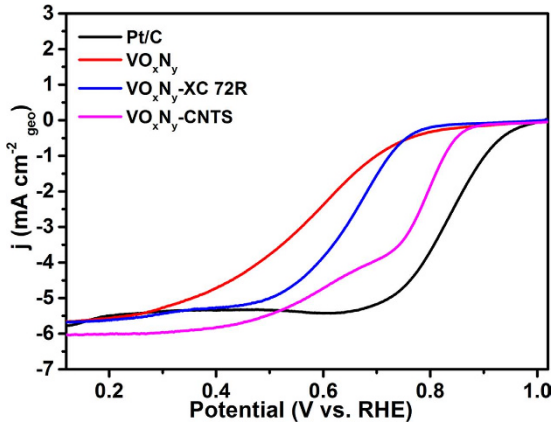

Figure 5. ORR activities of different VO_xN_y-based catalysts compared with Pt/C catalyst at 1600 rpm.

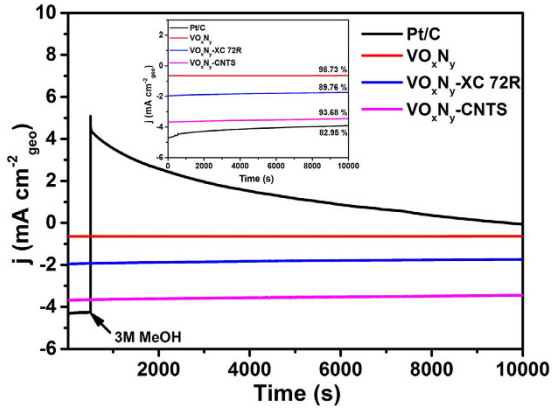

Figure 6. The chronoamperometric responses of different VO_xN_y-based electrodes as well as commercial Pt/C electrode with or without (insert) adding 3M MeOH at 500 s.

3M Methanol at 500 s. As shown in the inset of Fig. 6, the current densities of pure VO_xN_y electrode, VO_xN_y-Xc 72R electrode, VO_xN_y-CNTs electrode and Pt/C electrode remain 98.73%, 89.76%, 93.68% and 82.95% after 1000 s compared with the initial ones. The increased loss with the addition of XC 72R and CNTs can be attributed to the oxidation of carbon under dynamic potential conditions and high-oxygen environment[39,40]. Furthermore, unlike the instantaneous current density jump for Pt/C electrode due to the addition and the following electro-oxidation of methanol[41], all VO_xN_y-based electrodes exhibit superior methanol tolerance with negligible changes. In addition, the ORR performance in alkaline electrolyte of VO_xN_y-CNTs is also highly comparable to other widely studied non-precious electrocatalysts, such as 3D nitrogen-doped graphene aerogel-supported Fe_3O_4 nanoparticles (Fe_3O_4/N-GAs)[42], carbon nanotubes supported MnO_x hybrids (MnO_x/CNTs)[43], carbon-supported $CoSe_2$ nanocatalyst ($CoSe_2$/C)[44], cobalt and nitrogen-cofunctionalized graphene (Co-N-GN)[45] and Fe_2N-N-doped graphitic nanocarbons composite (Fe_2N-NGC)[46].

Discussion

To further understand the enhanced performance of VO_xN_y-CNTs catalysts with respect to VO_xN_y-XC 72R and pure VO_xN_y electrodes, cyclic voltammetry (CV) curves under both N_2- and O_2-saturated 0.1 M KOH electrolyte have been also recorded in Fig. 7. As can be seen, there are no obvious oxidation or reduction current peaks in all CV curves under N_2-saturated KOH solution differing from Fe-N/C catalysts which present redox couples due to the existence of instable metal ions[47]. Thus, this result also indicates the high electrochemical stability of VO_xN_y over the whole measured potential range. Meanwhile, significant ORR peaks can be observed for VO_xN_y-XC 72R (0.65 V vs. RHE) and VO_xN_y-CNTs (0.75 V vs. RHE) electrodes under the O_2-saturated condition compared with pure VO_xN_y electrode, which suggests the decreased overpotential and favorable charge transfer process for ORR[48,49]. Considering the above results of ORR polarization curves and chronoamperometric responses, VO_xN_y-CNTs composites exhibit a fascinating ORR activity and stability. As is well-known to all, ORR is a surface chemical process where the consumption of oxygen occurs on the surface of electrode materials. Therefore, the enhanced

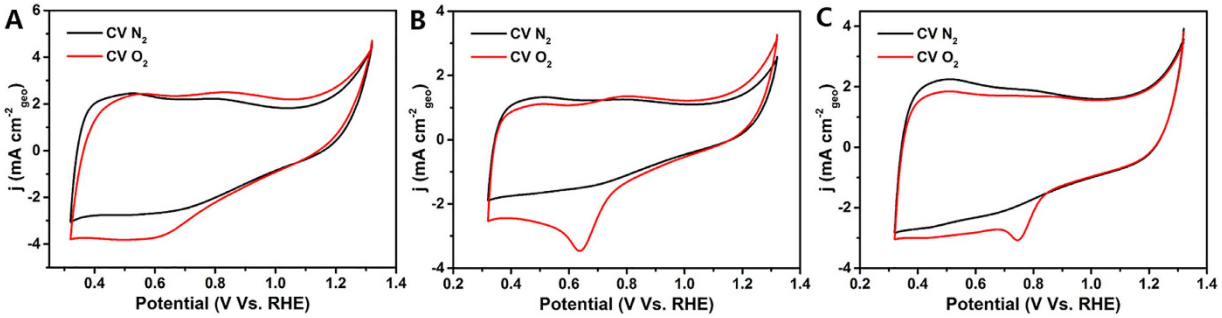

Figure 7. CV curves of VO_xN_y (A), VO_xN_y-XC 72R (B) and VO_xN_y-CNTs (C) as ORR catalysts in N_2/O_2-saturated 0.1 M KOH solution.

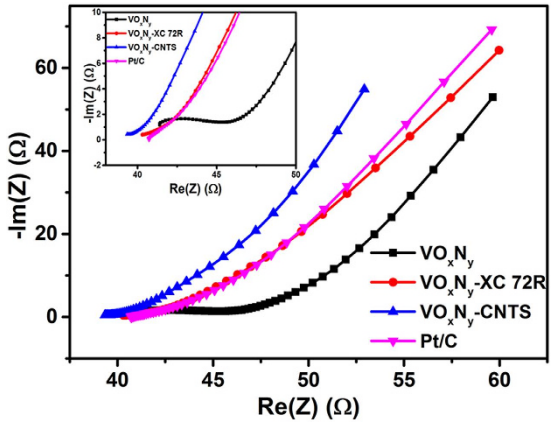

Figure 8. Nyquist plots corresponding to all referred electrodes in 0.1 M KOH solution from 100 kHz-1 Hz; The inset shows the low impedance region.

performance of VO_xN_y-CNTs composites is believed to be closely related to the surface chemical states: (i) the bond between the carbon and the nitrogen is favorable to elevate the ORR electro-catalytic activity; (ii) the surface VO_xN_y layer itself benefits the stability and tolerance of methanol.

On the other hand, the increased overall conductivity also contributes to the decrease of overpotential as demonstrated before[50]. To further monitor the different conductivity of Pt/C and all VO_xN_y-based electrodes, representative Nyquist plots of electrochemical impedance spectroscopy (EIS) are displayed in Fig. 8, where the high frequency region (see the inset) can be associated with the charge-transfer process as well as the properties of electrochemical reaction resistance and the low frequency straight lines relate to the properties of the diffusion process[51]. It is obvious that the initial resistances corresponding to the combination of solution resistance and the film resistance are 39.3, 40.2, 40.6 and 41.4 Ω for VO_xN_y-CNTs, VO_xN_y-XC 72R, commercial Pt/C and bare VO_xN_y electrodes respectively, which indicates the enhanced electrochemical conductivity due to the introduction of carbon support for VO_xN_y catalyst. Moreover, the apparent arc-shaped region for just bare VO_xN_y electrode which is relative to the charge-transfer resistance is also responsible for its large ORR overpotential. Thus, the highest overall conductivity of VO_xN_y-CNTs is beneficial to the higher ORR onset potential, i.e., the lower overpotential.

Furthermore, since the ORR is a multi-electron charge transfer reaction with two main possible paths in alkaline electrolyte: one is one step direct pathway, involving four electrons transfer to produce OH^- while the other one is two steps indirect pathway, involving two electrons transfer to produce HO_2^- and then the HO_2^- get another two electrons to transform into OH^-, rotating disk electrode (RDE) voltammetry (i.e. linear-sweep voltammetry, LSV) was performed in oxygen-saturated 0.1 M KOH solution at a scan rate of 5 mV/s with the rotation rate from 400 to 2000 rpm to gain further insight into the ORR process. Figure 9 shows that all VO_xN_y-based electrodes display elevated ORR current densities with the increase of rotation rate and VOxNy-CNTs perform best in view of all above three electrochemical parameters. In addition, the numbers of electrons transferred per oxygen molecule in ORR have been estimated on the basis of the well-known Koutechy-Levich (K-L) equation:

$$J^{-1} = J_K^{-1} + J_L^{-1} = J_K^{-1} + 5 \cdot (nFCD^{2/3}\nu^{-1/6}\omega^{1/2})^{-1} \quad (1)$$

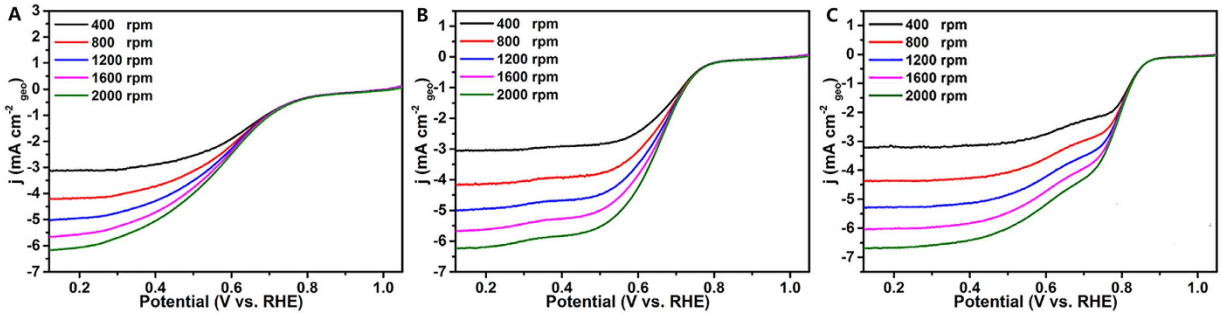

Figure 9. ORR polarization curves of VO_xN_y (A), VO_xN_y-XC 72R (B) and VO_xN_y-CNTs (C) as electrocatalysts in O_2-saturated 0.1 M KOH solution.

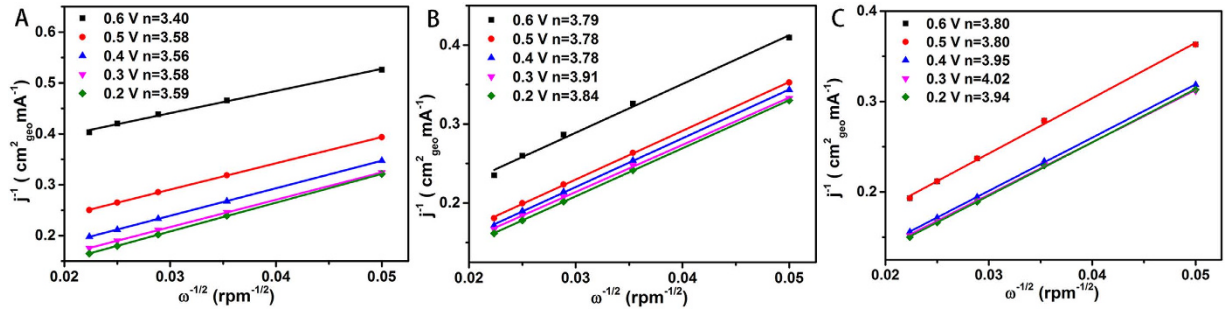

Figure 10. Koutechy-Levich (K-L) plots at different potentials for VO_xN_y (A), VO_xN_y-XC 72R (B) and VO_xN_y-CNTs (C) electrodes.

where J and J_K are the measured and kinetic current density, ω is the rotation rate in the form of rpm, n is the transferred electron number, F is the Faraday constant (96485 C mol^{-1}), C is the concentration of O_2 (1.2×10^{-6} mol cm^{-3}), D is the diffusion coefficient of O_2 (1.9×10^{-5} cm^2 s^{-1}), ν is the kinematic viscosity (0.01 cm^2 s^{-1}) in 0.1 M KOH solution[52]. As shown in Fig 10, the electron transfer numbers of VO_xN_y, VO_xN_y-XC 72R and VO_xN_y-CNTs electrodes at all selected potentials increase in sequence with the average electron transfer numbers of 3.54, 3.82 and 3.90 respectively. Thus, this results indicate that VO_xN_y-CNTs catalyst exhibits a direct 4-electron dominated reduction process. And consistent with the analysis of EIS measurements, the increased number of electron transferred also suggests that the addition of carbon support can facilitate the transfer of electron from the surface of catalysts to oxygen molecule.

In conclusion, we have successfully prepared novel porous VO_xN_y-CNTs nonocomposite which exhibits tremendous potential to be used as an appropriate non-noble ORR electrocatalyst with superior stability, excellent methanol-tolerance and competitive activity. Combining the results of electrochemical tests and structural characterizations, the porous structure among VO_xN_y nanoribbons can help the electrolyte and oxygen make adequate contact with the catalysts, the presence of CNTs as well as the formation of carbon-nitrogen bonds can further enhance the overall conductivity and reduce the overpotential for the motivation of ORR while the surface VO_xN_y layer itself benefits the tolerance of methanol.

Methods

Synthesis of VO_xN_y-CNTs nanocomposite. V_2O_5 nanobelts using as precursor were first prepared by a typical hydrothermal process, in which 2 mmol V_2O_5 powder was added into a mixture of 30 mL DI water and 5 mL H_2O_2 (30%) under vigorous stirring for 30 min to obtain a clear dark red solution before being transferred into a 50 mL of Teflon-sealed autoclave at 200 °C for four days. Meanwhile, 0.5 g of home-made CNTs (8–15 nm in diameter and 0.5–2 μm in length) were added into 50 mL of 98% H_2SO_4 and 14 mL of 65% HNO_3 solution, refluxed at 80 °C for 90 min and then recovered by centrifugation. Then, V_2O_5 nanobelts and acid-treated CNTs (V_2O_5: CNTs = 6: 4) were mixed together uniformly in certain DI water with the aids of ultrasonication and stirring. After the vacuum filtration, peeling off from the membrane and drying treatment, the obtained mixture powder was further annealed in NH_3 at 600 °C for 1 h with a ramping rate of 5 °C/min. Subsequently, the as-prepared sample was cooled down to room temperature under high purity nitrogen atmosphere. Moreover, pure VO_xN_y sample was obtained under the same conditions without the addition of CNTs.

Structure analysis of the VO_xN_y-based samples. Morphology and microstructure of the samples were characterized by powder X-ray diffractometry (XRD, X'pert PRO, Panalytical) using Cu Kα as radiation source, transmission electron microscopy (TEM, ARM200F, JEM) equipped with energy-dispersive X-ray spectroscopy (EDS). XPS measurements were carried out on an ESCALAB 250Xi spectrometer by Thermo Scientific with C 1s peak at 284.8 eV as an internal standard.

Electrochemical measurement of the VO_xN_y-based electrodes. All of the electroch-emical tests were performed on a three-electrode system (a glassy carbon electrode of 5 mm in diameter with a catalyst loading of 0.5 mg cm^{-2} as the working electrode, a Pt foil as the counter electrode and an Hg/HgO electrode as the reference electrode) using Autolab PGSTAT-204 and CHI 660E workstations. All potential values were calibrated with respect to reversible hydrogen electrode by $E_{RHE} = E_{Hg/HgO} + 0.92$ V. What's more, the preparation of VO_xN_y, VO_xN_y-XC 72R (60% VO_xN_y) and VO_xN_y-CNTs electrodes are similar to our previous works[23,53]. Cyclic voltammetry (CV) measurements were performed at a scan rate of 50 mv s^{-1} in N_2-/O_2-saturated 0.1 M KOH electrolyte. Rotating disk electrode (RDE) tests were conducted at different rotating speeds from 400 to 2000 rpm in O_2-saturated 0.1M KOH solution at a scan rate of 5 mv s^{-1}. The chronoamperometry responses (i-t curves) were carried on a constant voltage of 0.65 V in O_2-saturated 0.1 M KOH solution with or without adding 3M methanol at 500 s. Electrochemical impedance spectra (EIS) were measured from 1 Hz to 100 kHz with a potential amplitude of 10 mV.

References

1. Aricò, A. S., Bruce, P., Scrosati, B., Tarascon, J.-M. & Schalkwijk, W. V. Nanostructured materials for advanced energy conversion and storage devices. *Nat. Mater.* **4,** 366–377 (2005).
2. Dai, L. M., Chang, D. W., Baek, J.-B. & Lu, W. Carbon nanomaterials for advanced energy conversion and storage. *Small* **8,** 1130–1166 (2012).
3. Zhang, Q. F., Uchaker, E., Candelaria, S. L. & Cao, G. Z. Nanomaterials for energy conversion and storage. *Chem. Soc. Rev.* **42,** 3127–3171 (2013).
4. Li, Q., Cao, R. G., Cho, J. & Wu, G. Nanocarbon electrocatalysts for oxygen reduction in alkaline media for advanced energy conversion and storage. *Adv. Energy Mater.* **4,** 1301415–1301433 (2014).
5. Hu, C. G. *et al.* Tailored graphene systems for unconventional applications in energy conversion and storage devices. *Energ. Environ. Sci.* **8,** 31–54 (2015).
6. Chen, Z. W., Higgins, D., Yu, A. P., Zhang, L. & Zhang, J. J. A review on non-precious metal electrocatalysts for PEM fuel cells. *Energy Environ. Sci.* **4,** 3167–3192 (2011).
7. Liang, C. *et al.* Approaching high temperature performance for proton exchange membrane fuel cells with 3D ordered silica/Cs2.5H0.5PW electrolytes. *J. Mater. Chem. A* **2,** 753–760 (2014).
8. Li, J. R. *et al.* Highly ordered and periodic mesoporous Nafion membranes via colloidal silica mediated self-assembly for fuel cells. *Chem. Commun.* **49,** 6537–6539 (2013).
9. Pozo-Gonzalo, C. *et al.* Nanoporous transition metal oxynitrides as catalysts for the oxygen reduction reaction. *Electrochim. Acta* **103,** 151–160 (2013).
10. Zhong, H. X. *et al.* A novel non-noble electrocatalyst for oxygen reduction in proton exchange membrane fuel cells. *J. Power Sources* **164,** 572–577 (2007).
11. Ishihara, A., Doi, S., Mitsushima, S. & Ota, K. Tantalum (oxy) nitrides prepared using reactive sputtering for new nonplatinum cathodes of polymer electrolyte fuel cell. *Electrochim. Acta* **53,** 5442–5450 (2008).
12. Cao, R., Lee, J. S., Liu, M. L. & Cho, J. Recent progress in non-precious catalysts for metal-air batteries. *Adv. Energy Mater.* **2,** 816–829 (2012).
13. Wang, Y. D. *et al.* Several highly efficient catalysts for Pt-free and FTO-free counter electrodes of dye-sensitized solar cells. *J. Mater. Chem.* **22,** 4009–4014 (2012).
14. Das, B., Reddy, M. V. & Chowdari, B. V. R. X-ray absorption spectroscopy and energy storage of Ni-doped cobalt nitride, $(Ni_{0.33}Co_{0.67})N$, prepared by a simple synthesis route. *Nanoscale* **5,** 1961–1966 (2013).
15. Pande, P., Rasmussen, P. G. & Thompson, L. T. Charge storage on nanostructured early transition metal nitrides and carbides. *J. Power Sources* **207,** 212–215 (2012).
16. Balogun, M.-S. *et al.* Recent advances in metal nitrides as high-performance electrode materials for energy storage devices. *J. Mater. Chem. A* **3,** 1364–1387 (2015).
17. Zhou, X. P., Chen H. Y., Shu, D., He, C. & Nan, J. M. Study on the electrochemical behavior of vanadium nitride as a promising supercapacitor material. *J. Phys. Chem. Solids* **70,** 495–500 (2009).
18. Glushenkov, A. M., Hulicova-Jurcakova, D., Llewellyn, D., Lu, G. Q. & Chen, Y. Structure and capacitive properties of porous nanocrystalline VN prepared by temperature-programmed ammonia reduction of V_2O_5. *Chem. Mater.* **22,** 914–921 (2010).
19. Porto, R. L. *et al.* Titanium and vanadium oxynitride powders as pseudo-capacitive materials for electrochemical capacitors. *Electrochim. Acta* **82,** 257–262 (2012).
20. Cheng, F. K. *et al.* Preparation of nanocrystalline VN by the melamine reduction of V_2O_5 xerogel and its supercapacitive behavior. *Mater. Chem. Phys.* **131,** 268–273 (2011).
21. Shu, D. *et al.* Soft-template synthesis of vanadium oxynitride-carbon nanomaterials for supercapacitors. *Int. J. Hydrogen. Energ.* **39,** 16139–16150 (2014).
22. Huang, T. Z. *et al.* Hydrothermal synthesis of vanadium nitride and modulation of its catalytic performance for oxygen reduction reaction. *Nanoscale* **6,** 9608–9613 (2014).
23. Huang, K. *et al.* Novel VN/C nanocomposites as methanol-tolerant oxygen reduction electrocatalyst in alkaline electrolyte. *Sci. Rep-UK* **5,** 11351 (2015).
24. Yin, J. *et al.* Low-Pt loaded on a vanadium nitride/graphitic carbon composite as an efficient electrocatalyst for the oxygen reduction reaction. *Chem. Eur. J.* **19,** 13979–13986 (2013).
25. Lee, J.-S. *et al.* Metal-air batteries with high energy density: Li-air versus Zn-Air. *Adv. Energy Mater.* **1,** 34–50 (2011).
26. Zhu, Q.-L. & Xu, Q. Metal-organic framework composites. *Chem. Soc. Rev.* **43,** 5468–5512 (2014).
27. Ariga, K. *et al.* Layer-by-layer Nanoarchitectonics: invention, innovation, and evolution. *Chem. Lett.* **43,** 36–68 (2014).
28. Fu, Y. Q., Du, H. J., Zhang, S. & Huang, W. M. XPS characterization of surface and interfacial structure of sputtered TiNi fims on Si substrate. *Mat. Sci. Eng. A-Struct.* **403,** 25–31 (2005).

29. Dewangan, K. P. *et al.* V_2O_5 precursor-templated synthesis of textured nanoparticles based VN nanofibers and their exploration as efficient field emitter. *Vacuum* **109,** 223–229 (2014).
30. Yang, Z. H. *et al.* A facile route to VN and V_2O_3 nanocrystals from single precursor NH_4VO_3. *J. Alloy. Compd.* **420,** 229–232 (2006).
31. Fechler, N., Fellinger, T.-P. & Antonietti, M. Template-free one-pot synthesis of porous binary and ternary metal nitride@N-doped carbon composites from ionic liquids. *Chem. Mater.* **24,** 713–719 (2012).
32. Zhou, X. H. *et al.* Mesoporous coaxial titanium nitride-vanadium nitride fibers of core-shell structures for high-performance supercapacitors. *Acs Appl. Mater. Interfaces* **3,** 3058–3063 (2011).
33. Kartachova, O. *et al.* Evolution of the electrochemical capacitance of transition metal oxynitides with time: the effect of ageing and passivation. *J. Mater. Chem. A* **2,** 12940–12951 (2014).
34. Zhang, Y. J. *et al.* Biopolymer-activated graphitic carbon nitride towards a sustainable photocathode material. *Sci. Rep-UK* **3,** 2163 (2013).
35. Huang, K. *et al.* A facile route to reduced graphene oxide-zinc oxide nanorod composites with enhanced photocatalytic activity. *Powder Technol.* **257,** 113–119 (2014).
36. Wu, G. & Zelenay, P. Nanostructured nonprecious metal catalysts for oxygen reduction reaction. *Accounts Chem. Res.* **46,** 1878–1889 (2013).
37. Su, D. S., Perathoner, S. & Centi, G. Nanocarbons for the development of advanced catalysts. *Chem. Rev.* **113,** 5782–5816 (2013).
38. Yang, Z., Nie, H. G., Chen, X. A., Chen, X. H. & Huang, S. M. Recent progress in doped carbon nanomaterials as effective cathode catalysts for fuel cell oxygen reduction reaction. *J. Power Sources* **236,** 238–249 (2013).
39. Maass, S., Finsterwalder, F., Frank, G., Hartmann, R. & Merten, C. Carbon support oxidation in PEM fuel cell cathodes. *J. Power Sources* **176,** 444–451 (2008).
40. Avasarala, B., Moore, R. & Haldar, P. Surface oxidation of carbon supports due to potential cycling under PEM fuel cell conditions. *Electrochim. Acta* **55,** 4765–4771 (2010).
41. Lei, M. *et al.* Emerging methanol-tolerant AlN nanowire oxygen reduction electrocatalyst for alkaline direct methanol fuel cell. *Sci. Rep-UK* **4,** 6013 (2014).
42. Wu, Z.-S. *et al.* 3D nitrogen-doped graphene aerogel-supported Fe_3O_4 nanoparticles as efficient electrocatalysts for the oxygen reduction reaction. *J. Am. Chem. Soc.* **134,** 9082–9085 (2012).
43. Roche, I., Chaînet, E., Chatenet, M. & Vondrák, J. Carbon-supported manganese oxide nanoparticles as electrocatalysts for the oxygen reduction reaction (ORR) in alkaline medium: physical characterizations and ORR mechanism. *J. Phys. Chem. C*, **111,** 1434–1443 (2007).
44. Feng, Y. J. & Alonso-Vante, N. Carbon-supported cubic $CoSe_2$ catalysts for oxygen reduction reaction in alkaline medium. *Electrochim. Acta* **72,** 129–133 (2012).
45. Jiang, S., Zhu, C. Z. & Dong, S. J. Cobalt and nitrogen-cofunctionalized graphene as a durable non-precious metal catalyst with enhanced ORR activity. *J. Mater. Chem. A* **1,** 3593–3599 (2013).
46. Wang, L. *et al.* Ion-exchanged route synthesis of Fe_2N-N-doped graphitic nanocarbons composite as advanced oxygen reduction electrocatalyst. *Chem. Commun.* **49,** 3022–3024 (2013).
47. Feng, Y. J. & Alonso-Vante, N. Nonprecious metal catalysts for the molecular oxygen-reduction reaction. *Phys. Status Solid B* **245,** 1792–1806 (2008).
48. Yang, H. H. & McCreery, R. L. Elucidation of the mechanism of dioxygen reduction on metal-free carbon electrodes. *J. Electrochem. Soc.* **147,** 3420–3428 (2000).
49. Blizanac, B. B., Ross, P. N. & Markovic, N. M. Oxygen electroreduction on Ag (111): the pH effect. *Electrochim. Acta* **52,** 2264–2271 (2007).
50. Yi, J. Y. & Choi, G. M. The effect of mixed conductivity on the cathodic overpotential of $LaGaO_3$-based fuel cell. *Solid State Ionics* **175,** 145–149 (2004).
51. Liu, J. *et al.* Ultrathin Li_3VO_4 nanoribbon/graphene sandwich-like nanostructures with ultrahigh lithium ion storage properties. *Nano energy* **12,** 709–724 (2015).
52. Wang, S. Y., Yu, D. S. & Dai, L. M. Polyelectrolyte functionalized carbon nanotubes as efficient metal-free electrocatalysts for oxygen reduction. *J. Am. Chem. Soc.* **133,** 5182–5185 (2011).
53. Huang, K. *et al.* Novel graphite-carbon encased tungsten carbide nanocomposites by solid-state reaction and their ORR electrocatalytic performance in alkaline medium. *Electrochim. Acta* **174,** 172–177 (2015).

Acknowledgements

This work was financially supported by The National Basic Research Program of China (Grant No. 2013CB932901), Program for New Century Excellent Talents in University (NCET-13-0684, NCET-12-0911), Fund of State Key Laboratory of Information Photonics and Optical Communications (Beijing University of Posts and Telecommunications, P. R. China), and National Natural Science Foundation of China (Grant nos. 61574020, 51572032, 51402163, 61376018, 51272031, 61377097, 51472187).

Author Contributions

K.H., J.L., H.L.T. and M.L. conceived the idea, performed the experiments, analyzed and discussed data and wrote the paper; W.J.W., K.B., Y.K.L., R.Z. and Y.G.W. contributed to the synthesis and characterization of the samples.

Additional Information

Competing financial interests: The authors declare no competing financial interests.

How to cite this article: Huang, K. *et al.* Porous VO_xN_y nanoribbons supported on CNTs as efficient and stable non-noble electrocatalysts for the oxygen reduction reaction. *Sci. Rep.* **5**, 17385; doi: 10.1038/srep17385 (2015).